

Predicting disorder-order phase transitions in polymeric micelles

Glen A. McConnell and Alice P. Gast*

Department of Chemical Engineering, Stanford University, Stanford, California 94305-5025

(Received 21 March 1996)

The structure observed in concentrated polymeric micelles results from interactions between coronal chains that develop as micelles are brought to approach distances where the chains either compress or interdigitate. One powerful model for polymeric micelles comprises spherical particles with chains tethered to their core at a specified surface density. This treatment combined with self-consistent field theory provides an estimate of the pair interaction potential between micelles. These pair interaction potentials allow modeling of the structure and thermodynamic properties that depend on the overall micelle concentration. We perform neutron scattering experiments to measure the short-range correlations in the liquid, through the static structure factor $S(q)$, and compare these results with models that rely on a solution of the Ornstein-Zernike equation subject to a Rogers-Young closure. A description of the homogeneous liquid serves as the basis for employing density functional theory (DFT) to estimate the free energy of the solid. In this investigation, we use the modified weighted density approximation of Denton and Ashcroft [Phys. Rev. A **39**, 4701 (1989)] to estimate the free energy of the solid for each of our micellar systems to predict the liquid-solid phase transition. Although we experimentally observe transitions to face-centered-cubic (fcc) and body-centered-cubic (bcc) crystals depending on the length of the corona relative to the core, we only predict a simple liquid-fcc transition with the DFT method. The nature of the transition suggests a simple perturbation result using the hard sphere as the reference system. Despite the inability to predict the bcc lattice type, both DFT and hard-sphere models accurately predict coexistence over the entire range of our experiments. [S1063-651X(96)09811-X]

PACS number(s): 61.12.Ex, 61.25.Em, 83.70.Hq, 64.70.Dv

I. INTRODUCTION

The ability to predict phase transitions offers one of the most stringent tests for an accurate model of the thermodynamic properties of real systems. Much of this research focuses on combining model pair-interaction potentials with simulation methods such as Monte Carlo (MC) [2] or molecular dynamics (MD) [3,4]. The simulations yield exact results for model pair interactions preserving pairwise additivity [5], when finite size effects are considered.

One of the more important findings from simulations are the liquid-solid transitions occurring in systems having repulsive interaction potentials. Perhaps the most exhaustive investigation involves the inverse-power potentials where the potential energy $u(r)$ decays as r^{-n} [6–8]. This model potential spans long-range interactions such as the one-component plasma when $n=1$ to short-range interactions including hard spheres when n approaches infinity. Extensive studies of hard spheres show a temperature-independent first-order transition from liquid to face-centered crystal with a freezing volume fraction of 0.494 and a melting volume fraction ϕ_f , of 0.545 [9–11]. One unique feature of the inverse-power system is that their freezing transition is quite sensitive to the range of the repulsion [6]. In particular for $3 < n < 6$, the systems exhibit a stable body-centered-cubic (bcc) phase. Although Hoover, Young, and Grover concluded that the bcc phase was stable for $3 < n < 7$, Laird and Haymet [12] later showed that $n=6$ represents the largest value of n having a stable bcc phase. Although very few physical analogs exist for $3 < n < 6$, this pioneering work es-

tablished the perception that the range of the repulsion dictates the nature of the liquid-solid transition.

Another important soft-sphere potential is the Yukawa repulsion which corresponds to a screened Coulombic interaction $u(r) \approx \exp(-\kappa r)/r$, where $1/\kappa$ is the screening length. Robbins, Kremer, and Grest [13] performed MD simulations on this system and found stable body-centered-cubic (bcc) at low screening (small κ) and face-centered-cubic (fcc) at large κ . Charged colloidal particles forming fcc and bcc arrays can be successfully modeled with this potential [14].

Along with the Lennard-Jones potential [15,16], the Yukawa and inverse-power potentials represent the most thoroughly investigated model systems with complete phase diagrams. Although model potentials such as the finite step repulsion [17] and two-species soft core models [18] also have complete phase diagrams, they suffer from having limited physical analogs. The phase diagrams for other models, such as the Gaussian core studied by Stillinger and Weber [19,20], are still incomplete.

The computationally time-consuming nature of MD and MC simulations has propelled the field into less computationally intensive methods to predict thermodynamic properties. This includes liquid-state theories [21] based on integral equations and density functional algorithms [22] for predicting liquid-solid transitions. While these methods are approximate, they yield estimates of the thermodynamic properties approaching the accuracy of traditional simulation schemes. The density functional theory (DFT) has gained broad applicability because it relies on information about the homogeneous liquid to predict the free energy of the solid phase. The algorithm for relating the free energy of the solid to the uniform liquid defines both the method and its accuracy. Although several versions of density functional theory exist

*Author to whom correspondence should be addressed.

TABLE I. Aggregation numbers and length scales describing polymeric micelles comprising *d*-PS/PI diblocks in decane.

Polymer	f_A	R_c (Å) $P(q)$	R_T (Å) $S(q)$	R_h (Å) DLS	R_{eff} (Å) SCF	$\zeta/2R_c$ R-Y	Expt. lattice type	Lind. ratio Θ_L
15 K/15 K	80	74	63	195	185	0.111	bcc	0.171
19 K/8 K	270	116	100	184	189	0.139	fcc	0.139
20 K/10 K	235	117	103	220	207	0.133	fcc	0.157
33 K/22 K	335	150	136	362	329	0.100	fcc	0.137
36 K/36 K	245	142	141	467	432	0.084	bcc	0.189
44 K/22 K	420	204	197	484	401	0.125	fcc	0.184
40 K/40 K	90	106	78	296	275	0.100	bcc	0.182
45 K/45 K	130	137	145	450	472	0.090	bcc	0.165

[22], the weighted-density approximation of Curtin and Ashcroft [23] is both tractable and accurate; the modified weighted density approximation (MWDA) [1] provides close agreement with MD results for hard-sphere systems.

Laird and Kroll [24] applied several DFT methods to the inverse-power potential with mixed results. All methods were unable to predict a stable bcc phase, even under conditions where MD simulation results clearly show that the bcc phase is most stable. Only the weighted density approaches [1,23] provided a stable solution for all values of n in the inverse-power potential. They suggest that as the interaction increases in range, the DFT is unable to accurately map the interactions of the liquid onto the strongly correlated solid. In this case, the interaction potential extends over several lattice spacings and may explain the failure of the DFT to predict a stable bcc phase for long-range potentials despite the relatively accurate prediction of the hard-sphere transition.

With this in mind, the goal of this paper is twofold: (1) utilize pair-interaction potentials to understand the liquid-solid (fcc and bcc) transition observed in concentrated solutions of polymeric micelles, and (2) apply the density functional theory to determine its applicability in systems with repulsions extending over a finite range. We characterize the interactions between polymeric micelles with self-consistent field equations (SCF) for tethered-chain systems. Liquid state models offer predictions of the short-range correlations that are compared to small angle neutron scattering experiments at various liquid concentrations. The liquid-state theory models the thermodynamics of the homogeneous liquid through the radial distribution function. This information serves as the basis for predicting the liquid-solid transition using the MWDA method.

II. EXPERIMENT

A series of highly monodisperse, perdeuterated polystyrene-polyisoprene (*d*-PS-PI) diblock copolymers with varying block sizes and ratios were synthesized by a conventional, anionic polymerization technique [25]. The molecular weights for these diblock copolymers are reported in Table I. In all cases the polydispersity index is below or equal to 1.03. When these diblocks are suspended in decane, a solvent preferential for the polyisoprene block, the copolymers aggregate into spherical polymeric micelles comprising a dense core of *d* polystyrene and a diffuse corona of poly-

isoprene. Although the micelles coexist with free chains, the critical micelle concentration is so small (approximately 10^{-3} to 10^{-2} wt. % polymer) the solutions are dominated by micelles at all concentrations investigated here (ranging from 0.5 to 30 wt. %). More importantly, the micelles have a narrow range of aggregation number and can subsequently be treated as monodisperse spherical particles [26]. Portions of deuterated decane (Cambridge isotopes, 99% deuteration) and hydrogenated decane are mixed (0.107 mole fraction deuterated decane) to match the coherent scattering density of hydrogenated polyisoprene. As a result, the intensity measured from these suspensions are described by the scattering from constant density, spherical *d*-polystyrene cores and the spatial correlations developing at liquidlike concentrations.

The small angle neutron scattering experiments (SANS) were performed at beam line NG7 at the National Institute of Standards and Technology (NIST). Details about the beam-line facility are given elsewhere [27]. All intensity measurements were taken at an incident wavelength of $\lambda=7.00$ Å ($\Delta\lambda/\lambda=0.11$; full width at half maximum). The sample to detector distance was 11.0 meters giving a scattering vector $q[q=(4\pi/\lambda)\sin(\theta/2)]$, where θ is the scattering angle] causing q to range from 0.005 Å $^{-1}$ to 0.1 Å $^{-1}$. Data were placed on an absolute scale by cross referencing with the NIST silica standard using standard reduction techniques [28]. In addition, all experiments were performed at room temperature.

Experiments on monodisperse suspensions obey a simple form for the scattering intensity representing a product between the form factor and the structure factor [29]

$$I(q) = \rho P(q) S(q). \quad (1)$$

The form factor $P(q)$ accounts for the intramicellar interference describing the spherical shape of the particle and ρ is proportional to the number density of particles. The static structure factor $S(q)$ describes the interference arising from intermicellar interference, the short-range spatial correlations present in liquidlike micellar suspensions.

Characterizing these micellar suspensions at dilute concentrations (0.1 to 0.5 wt. % polymer) serves two purposes. Since no correlations between particles exists, the measured intensity depends only on the intramicellar interference

$$I(q) = \rho P(q), \quad (2)$$

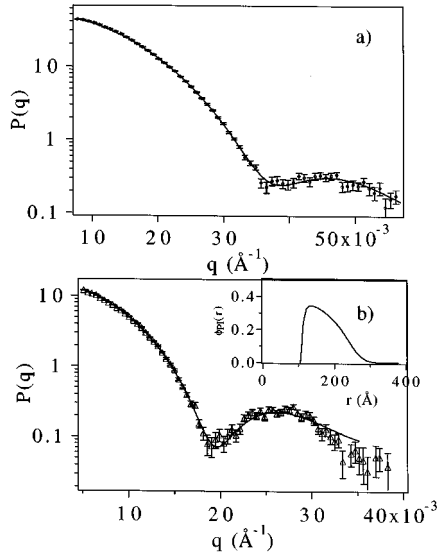


FIG. 1. (a) SANS form factor for micelles formed from *d*PS–PI 20 K–10 K diblocks in core contrast decane (achieved by mixing portions of *d*-decane and *h*-decane) at 0.5 wt. %. The lines correspond to the form factor for polydisperse spheres of core radius of 117 Å using a Schulz distribution with a polydispersity index Z of 90. (b) The form factor in PI contrast decane where only the micellar corona scatters. The line is a fit to the density profile from the SCF model illustrated in the inset.

allowing the separation of form and structure observed at higher concentrations, so that we can determine an experimental static structure factor for the liquidlike concentrations reported in this work. Secondly, we can model the form factor using constant density, solid-sphere models subject to a Schulz distribution function [30,31]. We present in Fig. 1(a) the form factor for *d*-PS–PI 20 K–10 K micelles in decane with the scattering contrast matched to the PI chains so that only the core shows; the line is the micellar core fit with the Schulz distribution solid sphere. Combining this with Zimm analysis [32] for absolute intensity allows the specification of core radius R_c and aggregation number f_A . We see no evidence of a virial contribution at low concentrations between 0.1% and 0.5%; thus we can use Zimm analysis to determine the aggregation number. The aggregation number does not seem to vary significantly with concentration. Our best evidence for this is the correspondence between missing peaks in the x-ray diffraction pattern for the ordered arrays and the minima in the form factors for the dilute micelles [26].

This information goes into our self-consistent field (SCF) calculations [33–35] of chains tethered to spherical cores [36–38]. These SCF models require the number of segments, N , for the solvated chain $N = M_{wPI}/(68K_r)$; here K_r is the Kuhn ratio, (1.57 [39] for PI in decane), the curvature relative to the PI segment length b , (R_c/b ; $b = 8.28$ Å) and the tethered-chain surface density [$f_A b^2/(4\pi R_c^2)$]. Given this information, we determine the PI concentration profiles from the SCF calculation. An illustration of the ability of the SCF model to depict the tethered PI layer is shown in Fig. 1(b), where we show the form factor for a dilute suspension of *d*-PS–PI 20 K–10 K micelles in decane with the scattering length density matched to the *d*-PS cores. The PI volume fraction profile used for the fit is shown in the inset. We then

calculate the pair interaction potentials by solving for the free energy for a pair of polymeric micelles as a function of their separation. Thus, in analogy with other colloidal systems, the influence of the PI corona is described in terms of the interaction potential between the cores. The interaction potential is zero for separations greater than the overall diameter of the micelle and the range depends on details associated with the core curvature, surface density, and degree of polymerization of the PI block. The pair potentials for the micelles formed from the diblocks stated in Table I were presented previously [40] and are used here for the liquid-state and density functional theories.

III. RESULTS AND DISCUSSION

A. Liquid-state theory

As described in Sec. II, scattering at dilute concentration provides sufficient characterization of each micellar system to utilize self-consistent mean field calculations to define the pair interactions between micelles. Within this model, we calculate the increase in free energy caused by compressing or interdigitating the coronal layers as a function of center-to-center separations. This provides a pair-interaction potential for the liquid-state theory, thus allowing the prediction of the thermodynamic state of the micellar suspensions observed at liquidlike concentrations.

We predict the structural and thermodynamic properties of a homogeneous solution by solving for the radial distribution function $g(r)$, at a specified density ρ , and our SCF pair interaction potential $u(R)$ [5,21]. The radial distribution function measures the local probability of finding another particle some distance from a reference particle. As a result, the radial distribution function represents a composite of direct and indirect particle interactions. These interactions are decomposed into separate interaction functions: a direct correlation function $c(r)$, describing the direct influence of one particle on any other, an indirect correlation function $\gamma(r)$, describing the influence of one particle on another through a third particle, and a total correlation function $h(r) = g(r) - 1$, including both direct and indirect contributions. Ornstein and Zernike developed a convolution integral equation relating all particle interactions [5]

$$\gamma(r_{12}) = h(r_{12}) - c(r_{12}) = \rho \int c(r_{23})h(r_{13})dr_3, \quad (3)$$

where the total correlation function $h(r)$, can again be represented by higher order direct and indirect correlation functions. Applying this method recursively generates an infinite series expansion in powers of the particle density that depend on higher order integrals of the direct and indirect correlation functions. Solving the Ornstein-Zernike equation requires a closure to relate two of the correlation functions to each other through the pair-interaction potential. Since the infinite series expansion represents the influence of specific clusters that can be expressed diagrammatically, the closure relations amount to assigning the cancellation between certain clusters. The quality of the closure then defines the accuracy of integral equations for describing liquid-state properties.

Although several closure relations exist to the Ornstein-Zernike equation, two of the most common include the Percus-Yevick (PY) [41,5,21]

$$g(r) = \exp[-\beta u(r)][1 + \gamma(r)] \quad (4)$$

and the hypernetted chain (HNC) [42,5,21]

$$g(r) = \exp[-\beta u(r)] \exp[\gamma(r)] \quad (5)$$

relations. The HNC relation appears to best describe the liquid-state properties of particles interacting through longer-range potentials such as the one-component plasma. The PY closure has effectively described the liquid-state properties of hard-sphere particles, a system with a short-range interaction potential. Thiele and Wertheim [43,44], however, demonstrated the limitations of the PY closure on hard-sphere systems by comparing the pressure calculated from the pressure equation

$$\frac{P}{kT} = \rho - \frac{\rho^2}{6kT} \int_0^\infty r \frac{\partial u(r)}{\partial r} g(r) 4\pi r^2 dr \quad (6)$$

with that calculated from integration of the compressibility equation

$$\frac{1}{kT} \frac{\partial P}{\partial \rho} = \frac{1}{1 + 4\pi\rho \int_0^\infty [g(r) - 1] r^2 dr} = \frac{1}{S(q=0)} \quad (7)$$

and demonstrating a lack of agreement observed at higher densities. Although Carnahan and Starling [45] arrived at a simple and accurate equation of state for hard-sphere systems, the lack of agreement in the pressure derived from two independent equations, referred to as thermodynamic inconsistency, is regarded as an important problem for liquid-state theories to overcome.

In recent years significant advances in integral theories have addressed the issue of thermodynamic consistency. One successful approach was developed by Rogers and Young [46]. This approach imposes a simple restriction of thermodynamic consistency with respect to one variable, the osmotic compressibility. The osmotic compressibility is calculated directly from Eq. (7) while that determined from the pressure Eq. (6) is

$$\begin{aligned} \frac{1}{kT} \frac{\partial P}{\partial \rho} &= 1 - \frac{\rho}{3kT} \int_0^\infty r \frac{\partial u(r)}{\partial r} g(r) 4\pi r^2 dr \\ &\quad - \frac{\rho^2}{6kT} \int_0^\infty r \frac{\partial u(r)}{\partial r} \frac{\partial g(r)}{\partial r} 4\pi r^2 dr. \end{aligned} \quad (8)$$

The Rogers-Young relation is a hybrid method mixing the PY and HNC closures such that the radial distribution function is given by

$$g(r) = \exp[-\beta u(r)] \left\{ 1 + \frac{\exp[\gamma(r)f(r)] - 1}{f(r)} \right\}, \quad (9)$$

where

$$f(r) = 1 - \exp(-\zeta r). \quad (10)$$

At $r=0$, $f(0)=0$ and the Rogers-Young recovers the PY closure relation. As r increases, $f(r)$ approaches unity and the closure relation approaches the HNC equation. In this man-

ner, the Rogers-Young relation uses the PY method at short distances and transforms to the HNC method at large separations at a rate determined by ζ . The value of ζ is adjusted to achieve thermodynamic consistency through agreement between the osmotic compressibility calculated from Eqs. (7) and (8). The resulting thermodynamic properties, including the radial distribution function, agree with molecular dynamics simulations for several model potentials [46–50].

Within this scheme we are combining an interaction potential calculated at discrete separations from SCF theory with the Rogers-Young closure to determine the radial distribution function for our polymeric micelles at liquidlike concentrations. To accomplish this goal, we modify Gillan's method [51], a numerical basis for calculating the radial distribution function from a discrete interaction potential. In this method, the indirect correlation function is broken into coarse and fine parts. The coarse part is expressed as a set of seven to ten orthonormal basis functions with unknown expansion coefficients. The fine part of the indirect correlation function is solved using Picard's method. We iterate until the differences are less than 10^{-10} or 10^{-20} . To achieve thermodynamic consistency, we employ Gillan's method at a particular value of ζ , calculate the osmotic compressibility from both the pressure and compressibility equation, and apply Newton-Raphson to generate a next best guess for ζ . We accept convergence when the compressibility calculated from both equations agrees to within 2%. Table I shows the values of ζ required to achieve thermodynamic consistency for the interaction potentials describing our micellar systems.

One feature of the convolution integral formalism is that the Fourier transform of the Ornstein-Zernike equation results in a simple algebraic expression

$$H(q) = C(q) + \rho C(q)H(q). \quad (11)$$

For a liquidlike suspension the theoretical structure factor becomes

$$S(q) = 1 + \rho H(q), \quad (12)$$

allowing direct comparison of the experimentally measurable structure factor with our liquid-state models. Figure 2(a) shows a comparison of experimentally measured structure factors with the model structure factors for micelles comprising diblocks with a 20 000 molecular weight *d*-polystyrene block and a 10 000 molecular weight polyisoprene block at various overall polymer concentrations. We extrapolate the model structure factors to wave vectors below those experimentally accessible because the value of $S(q=0)$ equals the inverse of the osmotic compressibility and we want to show how this varies with overall micelle concentration. These micelles have a mean aggregation number of 235 diblocks and a core radius of 117 Å. By measuring the scattered intensity at several concentrations we can test the validity of the SCF pair-interaction potentials. The model structure factor is obtained by adjusting the volume fraction and core radius via a Marquardt-Levenberg nonlinear regression subject to the Rogers-Young closure for the interaction potential. This thermodynamic radius R_T dimensionalizes the structure factor with respect to the scattering vector q . We find that the value of R_T converges to a consistent value with variations of less than 3% for all systems; however, in some

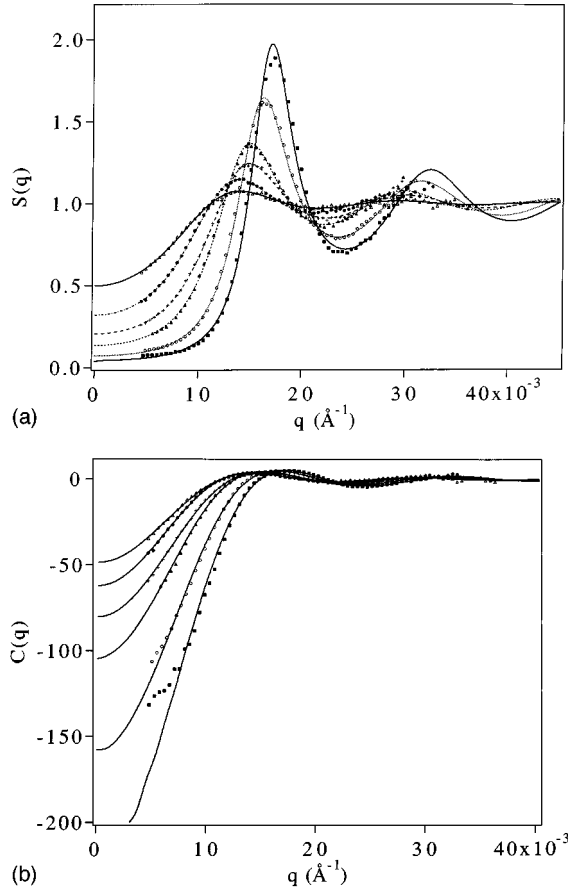


FIG. 2. (a) SANS static structure factors for micelles formed from *d*PS-PI 20 K-10 K diblocks in core contrast decane (achieved by mixing portions of *d*-decane and *h*-decane) at the following polystyrene core volume fractions (Φ_{PS}): $\Phi_{\text{PS}}=0.014$ (Δ); $\Phi_{\text{PS}}=0.024$ (\bullet); $\Phi_{\text{PS}}=0.036$ (+); $\Phi_{\text{PS}}=0.048$ (\triangle); $\Phi_{\text{PS}}=0.068$ (\circ); $\Phi_{\text{PS}}=0.088$ (\blacksquare). The lines correspond to fits using the SCF $u(r)$ potentials [40] subject to the Rogers-Young closure [46]. (b) The Fourier transform of the direct correlation function derived from Eq. (20) for experimental data compared with results from the Rogers-Young closure. The Fourier transform of the direct correlation function represents the homogeneous property influencing the MWDA result through Eq. (19).

micelles this value underpredicts the core radius by as much as 15% from our dilute characterization.

The thermodynamic core radius is the means of placing the interaction potential on a dimensional basis. One shortcoming of the SCF model is the presumptive nature of the interface. We idealized the polymeric micelles by determining core radii and tethering densities, and calculated pair interactions for spheres with polyisoprene chains tethered to perfectly sharp interfaces. In reality, the micelles are dense cores of polystyrene with some modest interfacial region for the effective tethering junction. According to our contrast match experiments, we expect this interfacial region to be on the order of 5 to 10 Å. Although the form of the interaction potential should be quite insensitive to the presence of the interfacial region, we expect the interface to directly influence the actual dimensional length of the pair-interaction potential. Thus we anticipate as much as 5% deviation between the thermodynamic core radius and our experimentally deter-

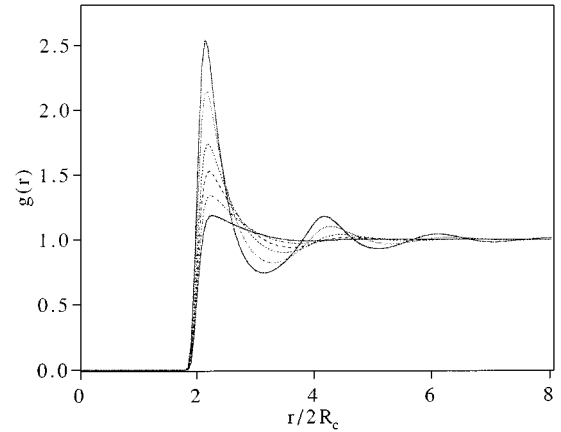


FIG. 3. Radial distribution functions for the micelles formed from *d*PS-PI 20 K-10 K diblocks in decane as a function of separation distance scaled upon the core diameter. The radial distributions result from using the SCF $u(r)$ [40] potentials subject to the Rogers-Young closure [46] for the polystyrene core volume fractions indicated in Fig. 1.

mined core radius from dilute solution scattering. If we correct the volume fraction to account for this variation, then we obtain excellent agreement between experimental and model core volume fractions.

The agreement between experimental and model structure factors establishes the accuracy for modeling the thermodynamic properties of the liquid state. In Fig. 3 we demonstrate the radial distribution functions for the micelles comprising 20 000-10 000 *d*-PS-PI diblocks at the respective concentrations. We can predict the pressure of the liquid state as a function of density with these distribution functions through Eq. (6). The density relates to the core volume fraction as $\Phi_{\text{PS}}=(\pi/6)\rho(2R_c)^3$. Owing to the different molecular weights of PI in each micellar system, the range of the repulsion is correspondingly altered, changing the core volume fractions where the pressure diverges, as shown in Fig. 4. Accurately predicting the pressure of the micellar liquid is necessary to estimate the excess free energy of the liquid. The total Helmholtz free energy is the sum of the excess

$$f_0^{\text{ex}}(\rho) = \int_0^\rho \left[\frac{P(\rho')}{\rho' kT} - 1 \right] d\rho' \quad (13)$$

and ideal free energy for the liquid

$$f^{\text{id}} = \ln(\rho) - 1. \quad (14)$$

B. Density functional theory

Density functional theory allows the prediction of the thermodynamic properties of an inhomogeneous solid based on information about the homogeneous liquid. This theory relates the second functional derivative of the free energy to the direct correlation function

$$\lim_{\rho_s \rightarrow \rho} -\beta \frac{\delta^2 F^{\text{ex}}}{\delta \rho(\mathbf{r}) \delta \rho(\mathbf{r}')} = c_0^{(2)}(\mathbf{r}, \mathbf{r}'). \quad (15)$$

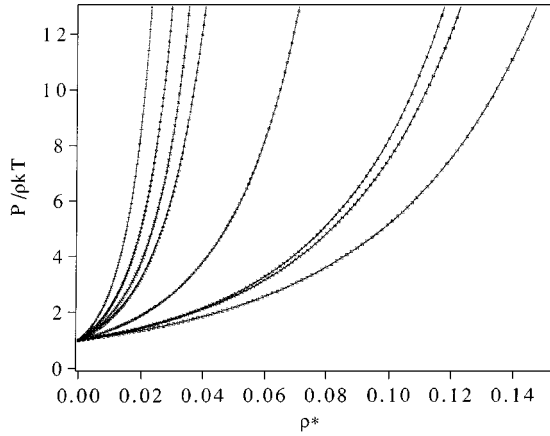


FIG. 4. The reduced pressure for each micellar liquid as a function of the reduced density. The pressure is determined by solving for $g(r)$ using Gillan's method [51] subject to the Rogers-Young closure [46] and applying Eq. (6). The symbols correspond to the micelles comprising the following d PS-PI diblocks in decane: 15 K-15 K (Δ); 19 K-8 K (\bullet); 20 K/10 K (\boxtimes); 33 K/22 K (\circ); 36 K/36 K (\times); 44 K/22 K ($*$); 40 K/40 K ($+$); 45 K/45 K (\diamond).

In the limit where the density approaches that of an actual liquid, Eq. (15) is exact. Although all density functional theories rely on Eq. (15) as their foundation, several methods have developed over the years to apply this relation to the inhomogeneous solid. The second order methods based on a truncated Taylor-series expansion offer simpler calculations but can be quite inexact and yield unphysical results [22,52]. The more successful weighted density approaches [1,23] both assume that the excess Helmholtz free energy of the inhomogeneous solid is equal to that of the liquid evaluated at some effective density

$$\frac{F^{\text{ex}}}{N} = f_0^{\text{ex}}(\rho). \quad (16)$$

The weighted density approximation (WDA) offers a more explicit theoretical formalism but is more computationally involved. The second version, known as the modified weighted density approximation (MWDA), gives a simpler procedure with essentially equivalent results to the original weighted density approximation.

The solid phase is represented by a sum of normalized Gaussians centered about their lattice sites R , such that

$$\rho_s(\mathbf{r}) = (\alpha/\pi)^{3/2} \sum_{\mathbf{R}} \exp(-\alpha|\mathbf{r}-\mathbf{R}|^2), \quad (17)$$

with the following Fourier components

$$\rho_G = \rho_s \exp(-G^2/4\alpha), \quad (18)$$

where G denotes the values of the reciprocal lattice vectors (RLV) for the solid [53]. The exact values of G depend on the lattice type and overall density of the solid phase. The localization parameter α determines the widths of the Gaussians and is a measure of the nonuniformity of the solid;

$\alpha=0$ corresponds to a uniform liquid and α approaching infinity signifies that the particles are fixed at their lattice positions.

Applying the MWDA largely amounts to satisfying the following relation:

$$\hat{\rho} = \rho_s \left[1 - \frac{1}{2\beta f_0'(\hat{\rho})} \sum_G \exp(-G^2/2\alpha) C(G; \hat{\rho}) \right], \quad (19)$$

where $C(q)$ is the Fourier transform of the direct correlation function evaluated at the corresponding values of the RLV for the proposed effective density. Since $C(q)$ is input into the density functional theory, it is important to model it accurately. One benefit of our scattering experiments is that we measure the static structure factor which is closely related to the Fourier transform of the direct correlation function [21]

$$C(q) = \frac{1}{\rho[1 - \rho S(q)]}. \quad (20)$$

We show a comparison of the experimentally determined Fourier transform of the direct correlation function with the model in Fig. 2(b). The ability to model the direct correlation function allows us to apply the MWDA to our micellar systems.

The value of $f_0'(\pi)$ is calculated from the pressure given by Eq. (6). Essentially, Eq. (19) yields an effective density for each value of α subject to one true density for the solid. The exact value of α becomes important for two reasons. First it determines the ideal contribution to the Helmholtz free energy

$$\frac{\beta F^{\text{id}}}{N} = \frac{3}{2} \ln(\alpha/\pi) - \frac{5}{2}, \quad (21)$$

such that the total Helmholtz free energy is a sum of the excess and ideal contributions and becomes a function of the localization parameter α . The total free energy, the sum of Eqs. (16) and (21), is then minimized with respect to α . Secondly, α is directly related to the mean-square displacement at freezing. The Lindemann parameter [54], defined as the square root of the mean-square displacement divided by the nearest neighbor distance, offers some insight about the mechanical stability of a solid. A critical value for the Lindemann ratio equal to approximately 0.13 was established empirically for the melting of a solid [21]. Table I lists the Lindemann ratios for our polymeric micelles using the MWDA approach. Although these values are slightly higher than the critical ratio, they represent reasonable estimates and verify the general applicability of the MWDA method to our polymeric systems.

The direct correlation function, excess free energy, and its first derivative serve as the necessary input for the MWDA prediction of the liquid-solid phase transition in polymeric micelles. The phase transition is determined by calculating the total Helmholtz free energy for each phase and using a double tangent construction to satisfy the equal pressure rule. Figure 5 shows the free energy predictions for the micelles comprising 20 K-10 K d -PS-PI diblocks. The free energies are a function of the polystyrene core volume fraction since

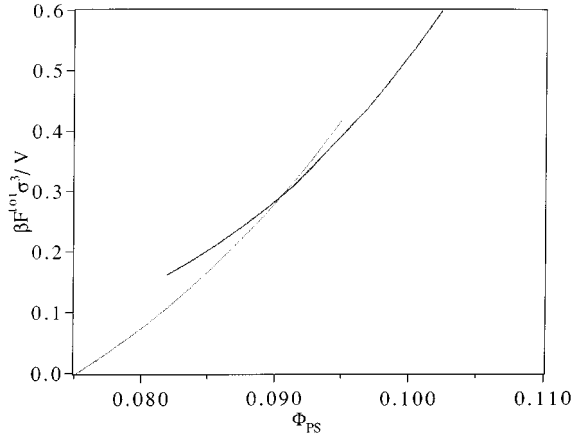


FIG. 5. Total free energy of the liquid (\cdots) and an fcc solid ($—$) for micelles comprising *d*PS/PI 20 K/10 K diblocks in decane detailing the liquid-solid transition using the MWDA of Denton and Ashcroft [1]. According to this model, we predict a freezing core volume fraction of 0.088 and a melting core volume fraction of 0.095.

the pair-interaction potential is nondimensionalized by the core radius. Specifying the interactions between micelles in this way establishes an analogy to charge stabilized colloids studied as a function of the bare colloid volume fraction where the electric double layer caused by the presence of counterions is responsible for the pair interaction potential. For micelles formed from suspending 20 K–10 K *d*-PS–PI diblocks in decane, the freezing volume fraction is 0.088 and the melting volume fraction is 0.095.

We applied this method to our micellar systems and are able to summarize our results in the phase diagram with experimental results and the DFT predictions in Fig. 6. In an earlier paper [26], we presented this semiquantitative phase diagram based exclusively on experimental results. We prepared several micellar systems at various core volume fractions and performed scattering experiments to determine their phase [26,40]. Each vertical column of data corresponds to experiments on a particular (PS–PI in decane) micellar system. The best way to summarize these results is to put the different molecular weight polymers on a common basis. We do this by using the PS core volume fraction as the concentration variable as it is independent of any model for overall micellar size. The interaction potential is then summarized by a measure of its range relative to the micellar curvature. We supplemented these experiments with small angle neutron, contrast matching experiments to determine the core radius and dynamic light scattering to specify the hydrodynamic layer thickness of the corona. The ratio of the layer thickness ($\langle L \rangle_h = R_h - R_c$) to the core radius (R_c) offers an experimental measure of the length scale of the repulsion relative to the curvature.

The phase diagram presented in this way splits into two regions where we observe a liquid-bcc transition at large range relative to curvature and the formation of fcc arrays at smaller range or larger core radius. The DFT method predicts the volume fraction for the phase transition for each system and this is denoted on the phase diagram by the (\times) symbols. Unfortunately, the DFT only predicts a liquid-solid transition favoring the formation of fcc crystals for all our micellar

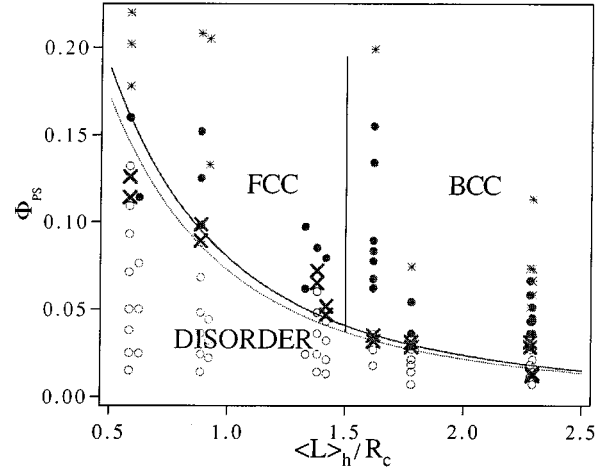


FIG. 6. Semiquantitative phase diagram for polymeric micelles detailing regions of order (\bullet) and disorder (\circ). The ($*$) symbols denote concentrations where diffraction data no longer corresponded to either a bcc or fcc lattice and may represent concentrations where micellar structure is modified. The lines represent the coexistence curves for the freezing and melting volume fractions as a function of hydrodynamic layer thickness to core radius ($\langle L \rangle_h / R_c$) according to Eqs. (24) and (25). The (\times) symbols indicate predictions of melting and freezing volume fractions determined by density functional theory for each micellar system investigated experimentally.

systems, even for those systems where the bcc phase is observed experimentally. Since Laird and Kroll [24] discovered that these DFT theories do not predict a stable bcc for inverse-power potentials, this raises suspicion about the accuracy of the DFT result.

To explore whether the fcc prediction is an artifact of the DFT method or accurately represents the stable phase based on simulation results, we compared these micelles to their thermodynamically equivalent inverse power potentials. Since the inverse-power potential is well understood and the formation of a stable bcc phase occurs for n less than 6, we decided to compare the liquid-state pressures as a function of effective density. In this case the effective density is determined by calculating the thermodynamic radius that causes the second virial coefficient in the pressure expansion to match

$$R_{\text{eff}} = \frac{1}{2} \left(3 \int_0^\infty \{1 - \exp[-u(r)/kT]\} r^2 dr \right)^{1/3}, \quad (22)$$

such that the effective volume fraction becomes

$$\Phi_{\text{eff}} = \frac{\pi}{6} \rho (2R_{\text{eff}})^3. \quad (23)$$

Plotting the reduced pressure as a function of effective volume fraction (Fig. 7) we can compare the pressures to that of the hard sphere ($n = \infty$). Increasing the range of the potential reduces the pressures from the hard-sphere result. One can see that for $n = 6$, the maximum inverse power for the formation of a stable bcc phase, the deviations are quite pronounced. Interestingly, our micellar systems all fall within a

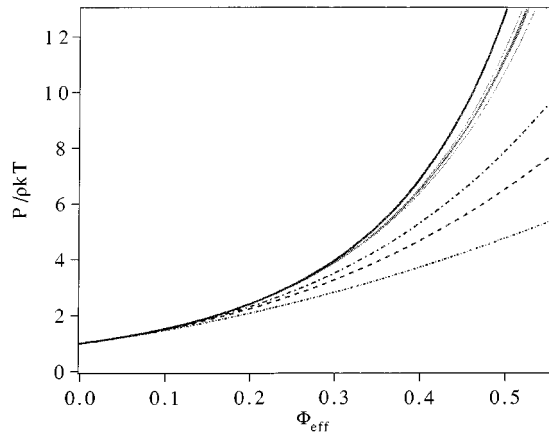


FIG. 7. Comparison of liquid pressures as a function of effective volume fraction for our micelles (\cdots) and the inverse power law systems: $n \rightarrow \infty$ (—), $n = 12$ (---), $n = 9$ (- - -), and $n = 6$ (\cdots).

narrow range between the inverse 12 potential and the hard-sphere result. Since this region is associated with liquid-fcc transitions, the DFT predictions may be accurate despite our observation of a bcc phase for some of our micellar systems.

Since we predict only the formation of an fcc phase, the phase diagram can be simply modeled in terms of hard-sphere perturbation theory with Eq. (22) defining the effective hard-sphere radius. The hard-sphere phase transition is first order with a freezing volume fraction of 0.494 and a melting volume fraction of 0.545. If we assume a simple relationship between the hydrodynamic radius and effective hard-sphere radius, the phase transition becomes

$$\Phi_{\text{PS}}^f = \frac{0.494}{B^3(1 + \langle L \rangle_h / R_c)^3} \quad (24)$$

and

$$\Phi_{\text{PS}}^m = \frac{0.545}{B^3(1 + \langle L \rangle_h / R_c)^3}, \quad (25)$$

where $B = R_{\text{eff}}/R_h$. The value of B appears to be relatively constant at 0.94 for all of our experimental micellar systems we show $B = R_{\text{eff}}/R_h$ in Fig. 8 for different values of $\langle L \rangle_h / R_c$. We are thus able to provide a simple and surprisingly accurate effective hard-sphere coexistence curve for our phase diagram in Fig. 6.

IV. CONCLUSION

Our understanding of the phase behavior of polymeric micelles benefits greatly from the predictions of pair interactions using self-consistent mean field equations for tethered chains. The range of the interaction potential is determined from the properties of the coronal layer offering medium range repulsions that dictate the nature of the liquid-solid transition. We have used these interaction potentials to predict the thermodynamic properties of the liquid state using integral equations. The Rogers-Young closure allows accurate prediction of the liquid state properties that are tested by monitoring the short-range correlations apparent in the micellar liquid through small angle scattering experiments. Fur-

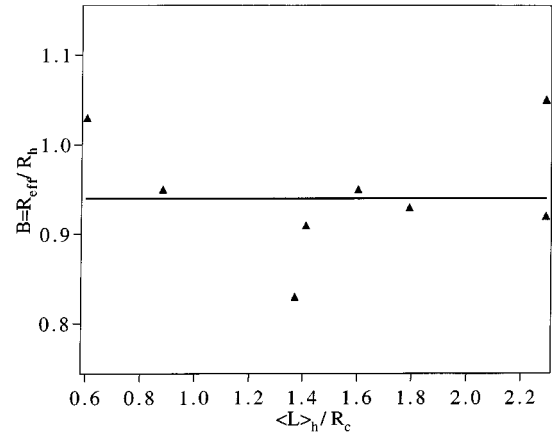


FIG. 8. A plot of $B (R_{\text{eff}}/R_h)$ as a function of the ratio of hydrodynamic layer thickness to core radius ($\langle L \rangle_h / R_c$). This plot demonstrates the constancy of B for our micellar systems and the applicability of Eqs. (24) and (25).

thermore, the static structure factor is related to the Fourier transform of the direct correlation function; this is the input necessary for the density functional theory. Application of the MWDA method predicts a liquid-solid transition favoring fcc micellar crystals for all systems studied experimentally by this group even for systems where diffraction results clearly demonstrate the formation of a bcc lattice [26].

The work of Laird and Kroll demonstrates the inability of DFT methods to predict the stable formation of the bcc phase for inverse-power potentials, even for conditions where molecular dynamics predict that the bcc phase is more stable. They suggested that the inability to accurately model the correlations over long distances explains the fallibility of density functional theory. This suggestion implies that DFT may predict a stable bcc phase for some interaction potential yet to be discovered. It was our hope to test the ability of the DFT theory to predict the ordering transition observed in our polymeric micelles particularly the formation of the bcc phase. We felt that because the interaction potentials in our polymeric micelles act over a finite distance specified by the micellar coronal chains that the DFT method might be able to describe the particle correlations more accurately than it does for the inverse-power potentials.

Our own investigations of the disorder-order transition with MWDA suggests that the method works reasonably well for our polymeric micelles. Comparisons of the reduced pressure with the effective density for our systems and the inverse-power potentials indicate that, in terms of the range of the micellar interaction potentials, the DFT theory appropriately predicts a stable fcc phase. The fact that we experimentally observe a stable bcc phase for some of our micellar systems implies that a more fundamental assumption may not be valid. Perhaps pairwise additivity for the potential energy is not preserved. We must remember that the pair-interaction potential is defined by the interaction of tethered, polymer chains and that increasing the concentration in these systems may adjust the thermodynamic behavior of the individual chains. Yet, despite the complex nature of the interactions in polymeric micelles, the application of pairwise models allow much insight into the nature of disorder-order

transitions in polymeric micelles including acceptable predictions of the coexistence curves.

Predicting the preference for lattice type (bcc or fcc) in these micellar systems still remains a challenging and intriguing aspect of research on the ordering of polymeric micelles. Since the experiments clearly demonstrate a preference for the lattice type based on a consideration of the length of the corona relative to core radius, we may have to resort to more complex models to delineate between micelles that favor the formation of bcc crystals over the fcc crystals. One possible approach is fully three dimensional SCF calculations of the free energy of micelles placed on either an fcc or bcc lattice. Although such a study may not provide liquid-

solid transition, it would allow a direct and accurate comparison of the free energy of the bcc solid relative to the fcc.

ACKNOWLEDGMENTS

This work was supported by NSF CTS-9413883. We acknowledge the support of the National Institute of Standards and Technology, U.S. Department of Commerce, in providing the facilities used in this experiment. We also wish to thank Min Y. Lin and Eric K. Lin for their help in the small angle neutron scattering experiments. We are especially indebted to Eric K. Lin for performing the SCF calculations that made this investigation possible.

-
- [1] A. Denton and N. Ashcroft, *Phys. Rev. A* **39**, 4701 (1989).
- [2] B. Berne, *Statistical Mechanics, Part A: Equilibrium Techniques* (Plenum, New York, 1977).
- [3] B. Berne, *Statistical Mechanics, Part B: Time Dependent Processes* (Plenum, New York, 1977).
- [4] H. Temperley, J. Rowlinson, and G. Rushbrooke, *Physics of Simple Liquids* (North-Holland, Amsterdam, 1968).
- [5] D. A. McQuarrie, *Statistical Mechanics* (Harper Collins, New York, 1976).
- [6] W. G. Hoover, D. A. Young, and R. Grover, *J. Chem. Phys.* **56**, 2207 (1972).
- [7] W. G. Hoover, S. G. Gray, and K. W. Johnson, *J. Chem. Phys.* **55**, 1128 (1971).
- [8] W. G. Hoover, M. Ross, and K. W. Johnson, *J. Chem. Phys.* **52**, 4931 (1970).
- [9] W. G. Hoover and F. H. Ree, *J. Chem. Phys.* **49**, 3609 (1968).
- [10] B. Alder and T. Wainwright, *J. Chem. Phys.* **27**, 1208 (1957).
- [11] B. Alder, W. Hoover, and D. Young, *J. Chem. Phys.* **49**, 3688 (1968).
- [12] B. B. Laird and A. Haymet, *Mol. Phys.* **75**, 71 (1992).
- [13] M. O. Robbins, K. Kremer, and G. S. Grest, *J. Chem. Phys.* **88**, 3286 (1988).
- [14] Y. Monovoukas and A. P. Gast, *J. Coll. Int. Sci.* **128**, 533 (1988).
- [15] A. Ladd and L. Woodcock, *Mol. Phys.* **36**, 611 (1978).
- [16] A. Ladd and L. Woodcock, *Chem. Phys. Lett.* **51**, 155 (1977).
- [17] D. A. Young and B. J. Alder, *J. Chem. Phys.* **70**, 473 (1979).
- [18] H. Ogura, H. Matsuda, T. Ogawa, N. Ogita, and A. Ueda, *Prog. Theor. Phys.* **58**, 419 (1977).
- [19] F. H. Stillinger and T. A. Weber, *J. Chem. Phys.* **68**, 3837 (1978).
- [20] F. H. Stillinger, *J. Chem. Phys.* **65**, 3968 (1976).
- [21] J. P. Hansen and I. R. McDonald, *Theory of Simple Liquids* (Academic, London, 1976).
- [22] Y. Singh, *Phys. Rep.* **207**, 351 (1991).
- [23] W. Curtin and N. Ashcroft, *Phys. Rev. A* **32**, 2909 (1985).
- [24] B. B. Laird and D. Kroll, *Phys. Rev. A* **42**, 4810 (1990).
- [25] S. Smith, *Polymer Solutions, Blends, and Interfaces* (Elsevier, Amsterdam, 1992), Chap. 2, pp. 43–64.
- [26] G. A. McConnell, A. P. Gast, J. S. Huang, and S. D. Smith, *Phys. Rev. Lett. A* **71**, 2102 (1993).
- [27] B. Hammouda, S. Krueger, and C. Glinka, *J. Res. Natl. Inst. Stand. Technol.* **98**, 31 (1993).
- [28] S.-H. Chen and T.-L. Lin, *Methods of Experimental Physics Part B* (Academic, New York, 1987), Vol. 23, Chap. 16, pp. 489–543.
- [29] M. Kotlarchyk and S.-H. Chen, *J. Chem. Phys.* **79**, 2461 (1983).
- [30] S. Aragon and R. Pecora, *J. Chem. Phys.* **64**, 2395 (1976).
- [31] P. Bartlett and R. Ottewill, *J. Chem. Phys.* **96**, 3306 (1992).
- [32] B. H. Zimm, *J. Chem. Phys.* **16**, 1093 (1948).
- [33] A. Dolan and S. Edwards, *Proc. R. Soc. London Ser. A* **343**, 427 (1975).
- [34] S. Milner, T. Witten, and M. Cates, *Macromolecules* **21**, 2610 (1988).
- [35] S. Milner, *Science* **251**, 905 (1991).
- [36] R. Ball, J. Marko, S. Milner, and T. Witten, *Macromolecules* **24**, 693 (1991).
- [37] N. Dan and M. Tirrell, *Macromolecules* **25**, 2890 (1992).
- [38] E. K. Lin and A. P. Gast, *Macromolecules* **29**, 390 (1996).
- [39] J. Brandrup and E. Immergut, *Polymer Handbook*, 3rd ed. (Wiley, New York, 1989).
- [40] G. A. McConnell, E. K. Lin, A. P. Gast, J. S. Huang, M. Y. Lin, and S. D. Smith, *Farad. Discuss.* **98**, 121 (1994).
- [41] J. Percus and G. Yevick, *Phys. Rev.* **110**, 1 (1958).
- [42] J. van Leeuwen, J. Groeneveld, and J. D. Boer, *Physica* **25**, 792 (1959).
- [43] E. Thiele, *J. Chem. Phys.* **39**, 474 (1963).
- [44] M. Wertheim, *Phys. Rev. Lett.* **10**, 321 (1963).
- [45] N. F. Carnahan and K. E. Starling, *J. Chem. Phys.* **53**, 600 (1970).
- [46] F. J. Rogers and D. A. Young, *Phys. Rev. A* **30**, 999 (1984).
- [47] B. D'Aguzzo and R. Klein, *Phys. Rev. A* **46**, 7652 (1992).
- [48] B. D'Aguzzo, *Phys. Scr.* **T49A**, 84 (1993).
- [49] H. S. Kang and F. Ree, *J. Chem. Phys.* **103**, 3629 (1995).
- [50] D. Heyes, *Phys. Chem. Liq.* **20**, 115 (1989).
- [51] M. Gillan, *Mol. Phys.* **38**, 1781 (1979).
- [52] B. B. Laird, *J. Chem. Phys.* **97**, 2699 (1992).
- [53] C. Kittel, *Introduction to Solid State Physics*, 5th ed. (Wiley, New York, 1976).
- [54] F. Lindemann, *Z. Phys.* **11**, 609 (1910).